Available online at www.sciencedirect.com
SCIENCE DIRECT®
Journal of Magnetic Resonance 165 (2003) 196–207
JMR Journal of Magnetic Resonance
www.elsevier.com/locate/jmr

Actively shielded multi-layer gradient coil designs with improved cooling properties

J. Leggett,[a] S. Crozier,[b] and R.W. Bowtell[a,*]

[a] *Magnetic Resonance Centre, School of Physics and Astronomy, University of Nottingham, Nottingham NG7 2RD, UK*
[b] *The School of Information Technology and Electrical Engineering, University of Queensland, Brisbane, Qld. QLD 4072, Australia*

Received 6 March 2003; revised 12 August 2003

Communicated by Joseph Ackerman

Abstract

In standard cylindrical gradient coils consisting of a single layer of wires, a limiting factor in achieving very large magnetic field gradients is the rapid increase in coil resistance with efficiency. This is a particular problem in small-bore scanners, such as those used for MR microscopy. By adopting a multi-layer design in which the coil wires are allowed to spread out into multiple layers wound at increasing radii, a more favourable scaling of resistance with efficiency is achieved, thus allowing the design of more powerful gradient coils with acceptable resistance values. Previously this approach has been applied to the design of unshielded, longitudinal, and transverse gradient coils. Here, the multi-layer approach has been extended to allow the design of actively shielded multi-layer gradient coils, and also to produce coils exhibiting enhanced cooling characteristics. An iterative approach to modelling the steady-state temperature distribution within the coil has also been developed. Results indicate that a good level of screening can be achieved in multi-layer coils, that small versions of such coils can yield higher efficiencies at fixed resistance than conventional two-layer (primary and screen) coils, and that performance improves as the number of layers of increases. Simulations show that by optimising multi-layer coils for cooling it is possible to achieve significantly higher gradient strengths at a fixed maximum operating temperature. A four-layer coil of 8 mm inner diameter has been constructed and used to test the steady-state temperature model.

PACS: 07.55.Db; 87.59.Pw

Keywords: Gradient coil; Shielding; High efficiency; NMR microscopy; Cooling

1. Introduction

Gradient coil design requires the consideration of a number of relevant parameters which affect the achievable performance. The coil inductance is important for fast imaging sequences since the shortest attainable gradient switching time is proportional to the inductance [1]. The power dissipated by the coil needs to be minimised both in order to allow the use of low power drivers and to minimise ohmic heating. The latter can be a particular problem for small and densely wound coils carrying large currents.

The degree of gradient homogeneity is important if good quality images are to be obtained; the received signal is interpreted assuming a linear field variation with position, so any deviation from this will cause spatial misrepresentation of voxel positions. Further, very large magnetic field gradients are required in a variety of NMR experiments. NMR microscopy [2] and pulsed gradient spin echo (PGSE) [3] experiments can particularly benefit from the availability of switchable gradients of more than $5\,\mathrm{T\,m^{-1}}$ strength. In NMR microscopy, large field gradients are needed to achieve fine resolution, particularly in the "diffusion-limited" regime, where diffusion under the read gradient is the dominant broadening mechanism [2]. In PGSE experiments, strong gradients in the field are necessary for the measurement of diffusion in low-mobility systems and

* Corresponding author. Fax: +44-115-9515166.
E-mail address: richard.bowtell@nottingham.ac.uk (R.W. Bowtell).

1090-7807/$ - see front matter © 2003 Elsevier Inc. All rights reserved.
doi:10.1016/j.jmr.2003.08.002

also allow the investigation of motion occurring on short timescales.

Access to such large gradients in small-bore systems is usually limited by the rapid increase in gradient coil resistance (R) with efficiency ($\eta = G/I$), which results from the reduction in usable wire diameter as the number of turns in a single layer, cylindrical gradient coil increases ($R \propto \eta^3$) [4]. Similar effects occur in coils constructed by cutting wire patterns in conducting layers because of the loss of conducting material with increasing number of cuts. Adopting a multi-layer approach to coil design, in which the coil windings are allowed to spread out in the radial direction, gives a more favourable scaling law [4], which allows larger gradients to be achieved at a given resistance and power dissipation.

However, although multi-layer coils dissipate less power at a fixed gradient strength than a conventional single-layer coil, the increased radial extent of the current distribution can cause problems for cooling the coil. If the overlying layers hinder heat flow sufficiently, it is possible that the internal temperature will be higher than in a single-layer coil, which dissipates more power. A pertinent question, therefore, is what temperature a coil will reach for a given current, and also whether it is possible to design a multi-layer coil so as to minimise the operational temperature.

A further notable design consideration relates to the magnetic screening of the gradient coils. Since MRI generally requires the gradient fields to be rapidly switched on and off, a temporally varying magnetic field is present [5]. This induces eddy currents in any conducting material in the vicinity of the gradient coil, such as the magnet's heat shields and the dewar walls. Such currents in turn generate time-varying magnetic fields which add to the primary imaging field, thus altering its linearity and time-dependence, potentially giving rise to image artifacts. Consequently, it is desirable to eliminate eddy currents by the use of a magnetic screen placed around the primary gradient coil so as to cancel the field in some external region. The perturbation to the primary field caused by the secondary coil can be accounted for in the design procedure such that within the internal region of interest, the two fields add to provide a linear field variation; outside the shield the two fields can be made to cancel [5,6].

Another requirement in gradient coil design is the generation of coils of finite length. Some methods produce a current distribution of effectively infinite axial length. This current is subsequently apodised, whereby it is multiplied by a function which tends to zero smoothly at the ends of the coil. This results in a current distribution of the same physical dimensions as the required coil former. However, the resulting characteristics will not be exactly the same as those of the current of infinite extent since the infinitely long distribution is the one which satisfies the coil design constraints. The first successful technique for generating finite length coils using a target field approach was that of Turner [7]. Other methods [8–12] are also able to accommodate the use of a finite length current distribution from the outset, thus eliminating the approximations inherent in appodisation.

Previously we have designed unshielded gradient coils [4,13] using a multi-layer variant of Carlson's harmonic minimisation technique [8]. Here, the technique is extended to the design and construction of length-constrained axial and transverse actively shielded multi-layer gradient coils, and coils with improved cooling properties.

2. Theory

2.1. Shielded gradient coils

In a multi-layer coil [4], the current distribution, $\mathbf{J}(\rho, \phi, z)$, is composed of N layers on cylinders of radii ρ_n. In each layer, the distribution can have axial and azimuthal components. Radial components are not considered here due to constructional difficulties associated with the resultant coil designs. For a longitudinal gradient coil, the axial component of $\mathbf{J}$ must be zero, whereas for a transverse coil, both components are required. The zero divergence of $\mathbf{J}(\rho, \phi, z)$ means that the axial and azimuthal current distributions are simply related [5,8] and the coil design can be fully specified in terms of $J_\phi(\phi, z)$ alone. The azimuthal current in the nth layer can be composed of a set of Q axial Fourier harmonics, weighted by the coefficients, λ_{nq}.

When designing a standard longitudinal gradient coil, the field, and consequently the current, needs to be antisymmetric in z. In this case, sinusoidal current harmonics are used and there is no azimuthal variation of the magnetic field or the current density. For a standard transverse gradient coil, the symmetry requires the current to be composed of cosinusoidal harmonics and there is additionally a cosinusoidal azimuthal dependence to the current density. For a non-symmetric gradient coil, both sets of harmonics are required [14].

In general, for a finite length coil of length $2l$, $|z| < l$, the azimuthal component of the required current distribution is given by

$$J_\phi(\rho, \phi, z) = \sum_{n=1}^{N} \sum_{q=1}^{Q} \delta(\rho - \rho_n) H(l - |z|) \times \lambda_{nq} \begin{Bmatrix} \sin(q\pi z/l) \\ \cos(q\pi z/l)\cos(\phi) \end{Bmatrix}, \quad (1)$$

where $H(\theta)$ is the Heaviside function, which takes a value of 0 for $\theta < 0$ and 1 for $\theta > 0$. The upper term in curly brackets corresponds to a z-gradient coil and the lower term to an x-gradient coil. The Fourier transformed current is

$$\tilde{J}_{\phi}^{m}(\rho,k)=\sum_{n=1}^{N}\sum_{q=1}^{Q}\delta(\rho-\rho_n)\times\lambda_{nq}\left\{\begin{array}{c}\mathrm{i}g_q^-(k,l)\delta_{m,0}\\ g_q^+(k,l)(\delta_{m,1}+\delta_{m,-1})\end{array}\right\},\tag{2}$$

where

$$g_q^{\pm}(k,l)=\mathrm{sinc}(kl+q\pi)\pm\mathrm{sinc}(kl-q\pi).\tag{3}$$

The total field produced, B_z, is the sum of the individual fields produced by each current harmonic in each layer, and at radii less than that of the innermost layer, ρ_i, is generally given by

$$B_z(\rho,\phi,z)=-\frac{\mu_0}{2\pi}\sum_{m=-\infty}^{\infty}\int_{-\infty}^{\infty}k\,\mathrm{d}k\,\mathrm{e}^{\mathrm{i}kz}\,\mathrm{e}^{\mathrm{i}m\phi}\times\int_0^{\infty}\rho'\,\mathrm{d}\rho'\tilde{J}_{\phi}^{m}(\rho',k)I_m(k\rho)K_m'(k\rho'),\tag{4}$$

A similar expression holds for radii greater than that of the outermost layer, ρ_o, but with the Bessel functions I_m and K_m interchanged. Using Eq. (2), Eq. (4) can be written as

$$B_z(\rho,\phi,z)=\sum_{n=1}^{N}\sum_{q=1}^{Q}\lambda_{nq}b_{nq}(\rho,\phi,z),\tag{5}$$

where the field component arising due to the qth current harmonic in the nth layer is given by

$$b_{nq}(\rho,\phi,z)=\frac{\mu_0}{\pi}\sum_{m=-\infty}^{\infty}\rho_n\int_0^{\infty}\mathrm{d}k\times k\left\{\begin{array}{c}\sin(kz)g_q^-(k,l)\delta_{m,0}\\ -\cos(kz)g_q^+(k,l)(\delta_{m,1}+\delta_{m,-1})\end{array}\right\}\times I_m(k\rho)K_m'(k\rho_n)\,\mathrm{e}^{\mathrm{i}m\phi}.\tag{6}$$

An expression for the inductance of the coil can be derived from the general relationship between the current distribution and stored energy [1,4], and an expression can also be derived for the total power dissipated by the coil [4].

In an approach similar to that of Carlson et al. [8], an optimal coil design is found by zeroing the differential of a functional with respect to λ_{nq}. As previously [4,13], the functional, Γ, comprises a weighted combination of the inductance, power, and the sum of the squares of the deviations of the field from its ideal value over a mesh of P constraint points within the region of interest where a linear field variation is desired.

The usual approach to screening a single layer coil is to place a secondary coil concentrically about the primary coil, thus introducing a second set of terms to all of the equations. However, here we already have multiple concentric layers of current, equally capable of acting as primary layers, shield layers, or some combination of the two, as determined by the current optimisation equations. All that is required, therefore, is to specify that the current distribution should produce a zero net field in a region outside the coil when field components produced by every harmonic in every layer are summed. Thus, the shielding is affected simply by the inclusion of an additional term in the functional equal to the sum of the squares of the deviations of the field from zero over a grid of U points outside the shield coil

$$\Gamma=\alpha P_{\mathrm{tot}}+\delta\sum_{p=1}^{P}\left(G\left\{\begin{array}{c}z_p\\ x_p\end{array}\right\}-B_z(\rho_p,\phi_p,z_p)\right)^2+\gamma\sum_{u=1}^{U}B_z(\rho_u,\phi_u,z_u)^2.\tag{7}$$

Inductance optimisation can also be included by adding in a weighted contribution from the total inductance. This was omitted in the work described here, since the focus was on designing small coils in which power dissipation is the limiting factor.

The $N\times Q$ equations resulting from minimisation of Eq. (7) are solved by Gaussian elimination. The relative importance of each constraint is set by the weighting factor (α, δ or γ) attributed to it. Thus, having evaluated the coefficients for the current harmonics, an optimised continuous current distribution can be obtained.

For an axial coil the azimuthal current density is integrated to yield the stream-function. Equally spaced contours in the stream-function define the locations of the current loops required to mimic the continuous current distribution.

For a transverse coil, the Fourier transform of the optimised two-dimensional current density is related to the two-dimensional Fourier transform of the stream-function, $S(\phi,z)$, by

$$\tilde{S}^m(k)=\frac{\tilde{J}_{\phi}^{m}(k)}{\mathrm{i}k},\tag{8}$$

where the tilde denotes the two-dimensional Fourier transform. The wire paths required to mimic the current distribution correspond to equally spaced contours of the current stream-function.

2.2. Heat flow equations

Consider conduction of heat from a cylindrical surface of area A_1 and temperature T_1, located at radius r_1, through a coaxial annulus having an outer boundary at a radius r_2, area A_2, and temperature T_2, followed by convection and radiation in parallel to a coolant of temperature T_3 (see Fig. 1).

For $r_1<r_2<r_3$, the total heat flow is given by

$$\dot{q}_{\mathrm{total}}=-UA\Delta T,\tag{9}$$

where $\Delta T=T_3-T_1$ and UA is effectively an overall heat conductance analogous to electrical conductance.

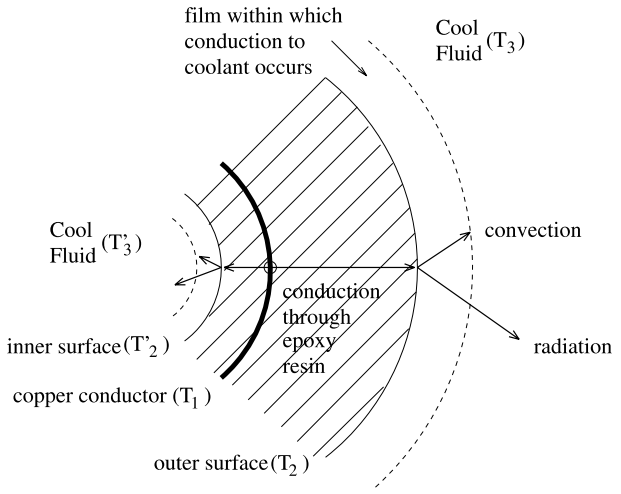

Fig. 1. Geometry of the coil showing relative locations of the coolant and electrically conductive layers of the coil.

As such, the total conductance from the source surface through the outer surface can be obtained by combining the conductances arising due to the individual heat transfer processes

$$\frac{1}{UA} = \frac{\Delta r_{12}}{A_{12}k} + \frac{1}{A_2 h_2}. \tag{10}$$

The first term arises from conduction through the coil, with

$$A_{12} = \frac{A_2 - A_2}{\ln(A_2/A_1)} \tag{11}$$

and

$$\Delta r_{12} = (r_2 - r_1) \tag{12}$$

The second term includes contributions from both convection and radiation at the coil surface.

Thus, the total heat removed from the surface at r_2 by outward heat flow is given by

$$\dot{q}_{\text{total}} = \{A_2(T_1 - T_3)\} \Big/ \left\{ \frac{A_2(r_2 - r_1)\ln(A_2/A_1)}{(A_2 - A_1)k} + \frac{1}{h_2} \right\}. \tag{13}$$

The same equations apply for $r_1 > r_2 > r_3$, but the subscripts for r and A need to be interchanged in the term A_{12} (Eq. (11)) describing conductive heat transfer. This also leads to a reversal of the subscripts in the first term of the bottom line in Eq. (13). The resulting expression describes the heat removed from the inner surface at r_2' by inward heat flow.

In an N-layer gradient coil, the properties of the copper layers can be labelled by two subscripts, so in place of T_1, we write $T_{1,n}$. Here the subscript "1" indicates that the temperature is that of a layer in the region containing the copper conductors. The additional subscript "n" refers to the specific layer number. The same labelling system can also be applied to both the radius and area in order to differentiate between the layers of the coil. The innermost layer is labelled layer "1" and the outermost is layer "N".

2.3. Optimisation of coils for cooling

Simple minimisation of the total power dissipated by a coil works well when designing single layer coils. However, the three-dimensional nature of the current distribution, and the additional potting material that is required, gives an added level of complexity to multi-layer coil design. In this case it may be desirable to modify the design procedure so that it is weighted to produce a coil having a current distribution formed so as to facilitate the removal of the heat generated. The more desirable wire positions are those nearest the coolant, i.e., nearest the coil surfaces, and furthermore, preferentially near to the surface with the higher heat transfer coefficient.

Given that it is easier to provide enhanced cooling, such as forced water cooling, at the outer rather than inner surface of the coil, the requirement for heat removal optimisation happens to be congruent with the requirements for good shielding performance; that is, a significant fraction of the current positioned near to the region to be shielded. However, gradient strength considerations favour placing all of the current as near to the gradient-field region of interest as possible, that is, near the inner coil surface. Thus, the requirements for cooling optimisation are not completely compatible with the other coil design requirements, so it can be expected that a price will have to be paid in terms of some of the other parameters in order to achieve enhanced cooling performance.

The technique adopted to design coils with improved cooling characteristics was to generate coils using the harmonic minimisation technique (v.i.), but with the slight modification that an additional multiplicative factor is applied to the current at each radius in the expression for the total power before insertion into the power term of the functional of Eq. (7). Since heat conduction through the coil from a radius $r_{1,n}$ depends upon $\Delta r_{12}/A_{12}$ in Eq. (10), it was decided that a suitable weighting parameter should also follow this form. As power dissipation in layers at larger distances from the coil surface requires a higher weighting in the functional, it can be seen that the required function should be inversely proportional to the conduction equation. Thus, the following weighting function was used

$$\text{wt}(n) = \frac{D(r_{1,n} - r_2')\ln(A_{1,n}/A_2')}{(A_{1,n} - A_2')} + \frac{(r_2 - r_{1,n})\ln(A_2/A_{1,n})}{(A_2 - A_{1,n})}. \tag{14}$$

Here, D is a function reflecting the relative values of the heat transfer coefficients for the inner surface at r'_2 and the outer surface at r_2, and n is the layer number.

A suitable function for D is one that varies smoothly from h_2/h'_2 at r'_2 to h'_2/h_2 at r_2. Since the multiplication factor varies from $x(=h_2/h'_2)$ to $1/x(=h'_2/h_2)$, this suggests the use of a logarithmic scale with the central value being unity. A suitable function, which varies the weighting logarithmically as the distance, ΔR, of the layer from the inner surface varies, is given by

$$D = C\exp\left[-\frac{\Delta R}{r_2 - r'_2}2\ln(C)\right], \tag{15}$$

with

$$C = \frac{h_2}{h'_2}. \tag{16}$$

The behaviour of this function is illustrated in Fig. 2. It can be seen that this function works regardless of whether h_2 or h'_2 is the larger, giving a small weighting for positions nearer the preferred surface and a larger weighting for positions further away.

By inserting $h_2 = h'_2$ the situation reduces to one of simple power minimisation with no preference for layer positioning. This occurs because the sum of heat resistances to two fixed end-points is being considered, and this will always be constant regardless of which intermediate point the resistance is measured from. Thus, basic power minimisation is a simplified version of the more complicated multi-layer, weighted, power minimisation.

2.4. Modelling heat flow

The model comprises layers of copper at which the temperature is to be calculated, separated by a heat conducting material (epoxy resin). The epoxy resin, being of considerably lower thermal conductivity (typically $k = 0.17$ to $0.87\,\mathrm{W\,m^{-1}\,K^{-1}}$ [15]) than the copper ($k = 401\,\mathrm{W\,m^{-1}\,K^{-1}}$ at 300 K [16]), will support a temperature gradient. The gradient across the copper layers will be negligible in comparison. We aim to model the steady-state condition. Consequently, at any given copper layer, the sum of heat entering the layer (both conducted and dissipated) has to equal the heat being conducted away from the layer.

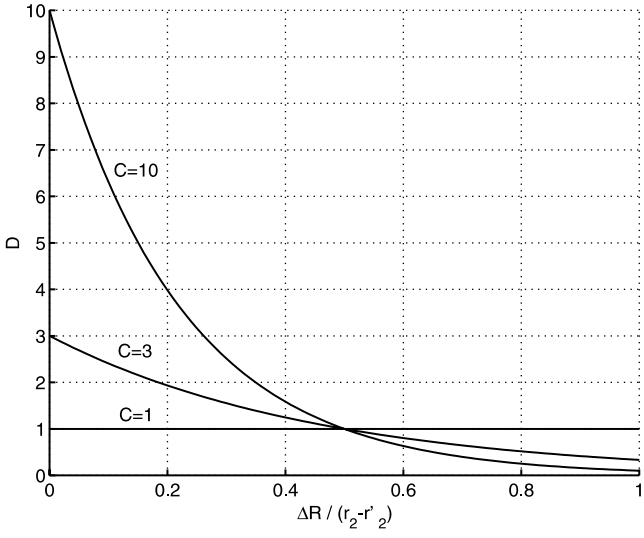

Fig. 2. Model used for the variation in the weighting function, D, with layer position, ΔR, when different heat transfer coefficients apply at the coil's inner and outer surfaces.

The objective is to find the equilibrium temperatures of the layers of the coil. To this end, a set of equations has been derived which can be used iteratively to refine an estimation of the equilibrium temperature distribution of the system. At equilibrium the following relationship holds for the outer surface

$$h_2A_2(T_3 - T_2) = \frac{(T_2 - T_{1,N})}{(r_2 - r_{1,N})}\frac{(A_2 - A_{1,N})}{\ln(A_2/A_{1,N})}k_{\mathrm{epoxy}} \tag{17}$$

which can be rearranged to give T_2 in terms of T_3 and $T_{1,N}$. A similar expression holds for the temperature of the inner surface, noting that the material between the wire and the surface is the inner former rather than epoxy.

If the heat-flow through the coil is to be modelled, expressions describing heat transfer at the individual copper layers are also required. These are found by consideration of energy conservation at each layer: the heat removed from each layer must equal the sum of the heat conducted into the layer and the heat dissipated in the layer by the current distribution therein. There are two different cases to consider: conduction between copper layers neighboured only by other copper layers and conduction from a copper layer, one side of which is neighboured by one of the coil surfaces.

For the first of the two cases listed above, the condition for equilibrium at the nth layer can be written as

$$P_n + \dot{q}_{n-1\to n} + \dot{q}_{n+1\to n} = 0, \tag{18}$$

where P_n is the ohmic heating due to the current flowing in the nth layer and $\dot{q}$ is the net heat flow between the two layers indicated by the subscripts. Writing this in full and rearranging to obtain an expression for the temperature of the nth layer in terms of its neighbours gives

$$T_{1,n} = [Z(n) + Z(n+1)]^{-1} \times \left\{\frac{I^2R_{1,n}}{k_{\mathrm{epoxy}}} + Z(n)T_{1,n-1} + Z(n+1)T_{1,n+1}\right\}, \tag{19}$$

where

$$Z(n) = \frac{1}{(r_{1,n} - r_{1,n-1})}\frac{(A_{1,n} - A_{1,n-1})}{\ln(A_{1,n}/A_{1,n-1})}. \tag{20}$$

For the case where one side of the layer is neighboured by a coil surface, the same approach is followed,

but an expression of the form of Eq. (13) has to be used for the conduction to the appropriate coil surface in order to account for the rate of heat removal from the surface. For the layer adjoining the outer surface of the coil, the temperature is given by

$$T_{1,N} = \left[\chi_o + k_{epoxy} Z(N)\right]^{-1} \times \left\{I^2 R_{1,N} + \chi_o T_3 + k_{epoxy} Z(N) T_{1,N-1}\right\}, \quad (21)$$

with

$$\chi_o = A_2 \Big/ \left\{ \frac{A_2 \ln\left(A_2/A_{1,N}\right)(r_2 - r_{1,N})}{k_{epoxy}(A_2 - A_{1,N})} + \frac{1}{h_2} \right\} \quad (22)$$

and for the layer nearest to the inner coil surface

$$T_{1,1} = \left[\chi_i + k_{epoxy} Z(2)\right]^{-1} \left\{I^2 R_{1,1} + \chi_i T_3' + k_{epoxy} Z(2) T_{1,2}\right\}, \quad (23)$$

with

$$\chi_i = \{A_2'\} \Big/ \left\{ \frac{A_2' \ln\left(A_{1,1}/A_2'\right)\left(r_{1,1} - r_2'\right)}{k_{former}\left(A_{1,1} - A_2'\right)} + \frac{1}{h_2'} \right\} \quad (24)$$

In Eqs. (21)–(24), the primed variables with "2" and "3" subscripts refer to the inner surface and coolant, respectively, as opposed to the equivalent unprimed variables which refer to the outer surface and coolant.

For an N-layer coil, a set of N coupled equations can be generated and then solved simultaneously. These equations require a knowledge of the resistance of each layer in order to calculate the power dissipated therein. The resistance of each layer can be calculated from the length, cross-sectional area, and resistivity, ρ, of the wire used

$$R = \frac{\rho l}{A}. \quad (25)$$

However, the resistivity is dependent on the wire temperature. At 293 K copper has a resistivity of $1.673 \times 10^{-8}\,\Omega\,m$ [17], and at this temperature the coefficient of variation of the resistivity with temperature, $d\rho/dT$, has a value of [17] $3.93 \times 10^{-3}\,K^{-1}$.

3. Method

Coil design programs employing the expressions described in the theory section were implemented using Fortran77. The magnetic field, B_z, produced by the discretised coil designs was calculated using computer programs which divided the current paths into small elements that were then fed into a field calculation based upon the elemental Biot–Savart expression.

The multi-layer approach is most advantageous for the design of coils of small diameter, where the limiting factor is generally the coil resistance rather than the inductance. We therefore did not concern ourselves with optimisation of the inductance. In designing coils, as low a dissipated power as possible was sought, whilst limiting deviations from gradient linearity to less than 5% within the specified ROI.

The first coil designed was a four-layer z-coil which was subsequently constructed and used to test the coil cooling model. The coil was designed with 2.3 mm layer spacing and the first layer was located at a radius of 9.70 mm. A large layer spacing was needed to allow mounting of temperature sensors at each layer. The internal region of interest within which the field deviation from a perfect gradient was to be less than 5% was defined to be a cylinder whose diameter was 0.55 times that of the first layer, with a total length equal to 0.54 times the first layer diameter. The total coil length was constrained to be twice the inner layer diameter. Shielded coils were designed using ratios for the outer to inner cooling coefficients of $C = 1$ (i.e., unweighted), $C = 3$, and $C = 10$. The number of wires in the inner layer was chosen such that the closest conductor spacing just allowed the use of wire of total diameter 0.32 mm (comprising 0.28 mm diameter copper covered by an 0.02 mm enamel layer). This determined the current step in the stream-function for the positioning of the wires, and the same current step was used in all subsequent layers. By this method, the maximum number of wires, and thus maximum possible efficiency using the gauge of wire intended for constructional purposes, was achieved.

For comparison, unscreened four-layer coils of identical geometry were also designed using each of the cooling coefficient ratios in order to assess the effect of including shielding on the coil performance. It was found, as discussed later, that higher values of C led to an enhanced level of shielding, but also to a slightly higher coil inductance. Using $C = 3$ seemed to provide the best compromise between inductance and shielding requirements, so this value was adopted for the coil that was built. The $C = 1$ and $C = 10$ coils were then re-designed to criteria set by the characteristics of the $C = 3$ coil. That is to say, the coils were designed with the same homogeneity constraints and the number of wires was chosen so as to match the resistance of the $C = 3$ coil. The coils were made as efficient as possible by using the largest number of turns which satisfied the resistance constraint. The wire diameter was set by the minimum wire spacing in the region of the coil with the highest current density (allowing for an 0.02 mm coating of enamel on the wire).

The four-layer, $C = 3$, z-gradient coil was constructed around a fibre-glass former of internal diameter 8.0 mm and external diameter 10.0 mm. Grooves were machined into the former to accept the first layer of wires, centred at a radius of 9.70 mm. A temperature sensor was glued to the wires approximately centred at the region of highest current density. The sensor covered most of the layer's windings and so would effectively have measured an average layer-temperature in the vicinity of the wires.

The assembly was then set in a layer of Araldite epoxy resin (kit K3600). Once it had set, the epoxy was turned down to the radius of the next layer. A new set of grooves was milled into its outer surface to accept the next set of wires, and a temperature sensor was subsequently placed above the bedded conductors. This procedure was repeated until all of the layers had been laid. A final covering layer of epoxy was then used to seal the outer layer. The finished coil is shown in Fig. 3.

During construction it was decided that in order to enhance the heating effect, thus emphasising the temperature gradients and giving larger measurable temperature differences, wire with half the cross-sectional area of that originally intended would be used (total diameter 0.24 mm including a 0.02 mm enamel layer). The effect of this was to double all of the coil resistances, and thereby double the power dissipated in the coil at any given current. However, the coil performance was not otherwise altered in any way.

The coil was tested by energising the windings with various currents at 100% duty-cycle. The coil was cooled by both natural convection of air and radiation at the outer surface. The 8.0 mm diameter cylindrical bore of the coil was sealed at both ends so there were no net convection currents at the inner surface. However, there may still have been localised air currents acting to even out any surface temperature variations arising from the inhomogeneity of the current distribution within the layers. Further, once the air in the cavity had come to thermal equilibrium with the coil's inner wall, there would also have been no net radiation losses from the inner surface. The coil was allowed to thermally equilibriate with its surroundings, then temperature measurements were made on each layer and on the surrounding air.

The measured coil layer temperatures were fitted to the thermal model to test its performance. To do this, the inner surface heat transfer coefficient was set to zero in the model. The condition that at equilibrium the coil's inner surface and the air within the bore cavity must be at the same temperature as the inner layer of windings was also imposed to account for the closed coil bore. This meant that the temperature gradient from the inner layer occurred in the positive radial direction only.

The only two parameters needed for fitting were the thermal conductivity of the epoxy resin and the heat transfer coefficient of the outer surface. However, the surface heat transfer coefficient incorporates components of convectional and radiational heat-loss. As such, any value determined will only be valid at the particular temperatures at which it was fitted. This is due to the differing temperature dependences of the two heat transfer mechanisms [18]. In practice, the value will not change significantly at low temperatures due to the relatively small contribution of the radiation component. Having varied the combinations of these two parameters to obtain a good fit for the temperatures of all four layers, the next step was to compare the performance of the coils designed using differing degrees of thermal weighting. To do this, the temperatures of the $C = 1$, $C = 3$, and $C = 10$, four-layer, z-coils were modelled assuming 100% current duty cycles and identical cooling conditions as occurred during aquisition of the experimental data.

A further experiment conducted on the coil was to measure the field generated at a number of axial positions immediately outside the four-layer shielded coil. This was done using a search-coil whilst driving the gradient coil with a 1 kHz sinusoidal wave-form. In order to assess the shielding, identical measurements were also made with current flowing through the inner layer of the coil alone.

A set of shielded and unshielded x-gradient coils was also designed with $C = 1$, $C = 3$ and $C = 10$ using the same criteria. The only difference with this set of coils was that the coil length was set to be four times the diameter of the first layer: the extra length being necessary in order to allow for the return paths of the windings, which are not required in the z-coil.

In order to assess the variation of coil performance with number of layers, a further set of coils was designed. Shielded and unshielded z- and x-gradient coils with 5 and 8 layers were produced, both in weighted ($C = 3$) and unweighted ($C = 1$) form. In order to effect

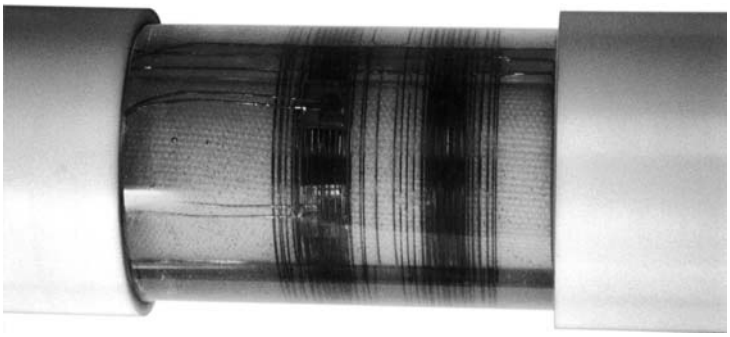

Fig. 3. A photograph of the constructed coil showing the windings and temperature sensors through the epoxy resin.

a fair comparison, all coils were designed so that their current distributions were evenly distributed over the same volume as that occupied by the previous four-layer coils (between radii of 9.70 and 16.60 mm). That is to say, the outer and inner layers occupied the same radial locations for all coils and the remaining layers were equally spaced in between. As before, the x- and z-coil half-lengths were 4 and 2 times the inner radius, respectively, and the same ROI was used as in the four-layer coils. The numbers of wires in each coil was adjusted to give a resistance of about 2 Ω. Again, each coil was made as efficient as possible by using the largest diameter wire that did not give rise to overlap with neighbouring conductors at the closest wire-spacing, but in this case no allowance was made for the presence of an enamel coating.

Conventional two-layer screened coils comprising a primary and a screen were also designed to these specifications. The layers were positioned to coincide with the innermost and outermost layers of the four-layer coils. These positions were adopted since this is where most of the current distribution will be situated in order to optimise the gradient efficiency (through proximity of primary current distribution to ROI) and shielding (through proximity of shielding current distribution to shielded region).

4. Results

4.1. Simulations

Table 1 summarises the performance of the final four-layer, z-coil designs. The average shielding values were calculated by taking the ratio of the RMS field strengths of the screened and unscreened coils. These were evaluated over an array of points equally distributed between radii of 0.0194 and 0.0251 m, and axial distances of 0 and 0.043 m. The results indicate that the presence of the shielding term in the functional acts to significantly attenuate the external magnetic field. Inspection of the distribution of wires across the layers indicates that inclusion of the screening condition leads to a reduction of the relative number of turns in the middle layers of the coil. It can also be seen that the inclusion of screening leads to a significant reduction in the coil efficiency at fixed resistance.

Adding in the cooling weighting with a higher coefficient at the outer surface can be seen to move even more of the current distribution away from the inner layers, and the effect is more pronounced at higher values of C. The coil efficiency does not change significantly with C, while the inductance rises slightly at higher C-values. However, the shielding is markedly improved for $C = 10$. This is due to a higher proportion of the current flowing in the outer layers which provide the screening, and hence a more accurate representation of the shielding current is yielded upon discretisation. Similar trends can be observed by studying Table 2 which shows the equivalent coil parameters for the four-layer x-coils.

Fig. 4 shows the variation of the temperature of the innermost (hottest) layer of the set of four-layer x- and z-coils as a function of current under identical cooling conditions (i.e., assuming the same ambient temperature and the same ratio of cooling coefficients to hold at the inner and outer surfaces in each case), operating with 100% duty cycle. The upper line of the z-coil data-set

Table 1
Summary of key parameters for shielded (sh) and unshielded (u/sh), axial, multi-layer gradient coils incorporating enhanced cooling

	u/sh, $C = 1$	sh, $C = 1$	sh, $C = 3$	sh, $C = 10$
Average shielding	—	4.869%	2.287%	0.576%
Efficiency ($T\,m^{-1}\,A^{-1}$)	0.319	0.176	0.175	0.185
Inductance (μH)	120.88	32.57	33.61	39.51
Resistance (Ω)	2.180	2.243	2.228	2.060
No. of wires/layer	26, 17	28, 10	23, 13	21, 16
	12, 8	2, 8	6, 10	10, 14
Wire diameter (μm)	350	302	320	361

Table 2
Summary of key parameters for shielded (sh) and unshielded (u/sh), transverse, multi-layer gradient coils incorporating enhanced cooling

	u/sh, $C = 1$	sh, $C = 1$	sh, $C = 3$	sh, $C = 10$
Average shielding	—	1.980%	1.056%	0.189%
Efficiency ($T\,m^{-1}\,A^{-1}$)	0.217	0.131	0.131	0.133
Inductance (μH)	123.89	36.39	36.99	43.29
Resistance (Ω)	2.338	2.142	2.060	2.107
No. of wires/layer	18, 12	23, 9	21, 11	19, 14
	9, 6	1, 8	2, 11	8, 14
Wire diameter (μm)	385	364	384	419

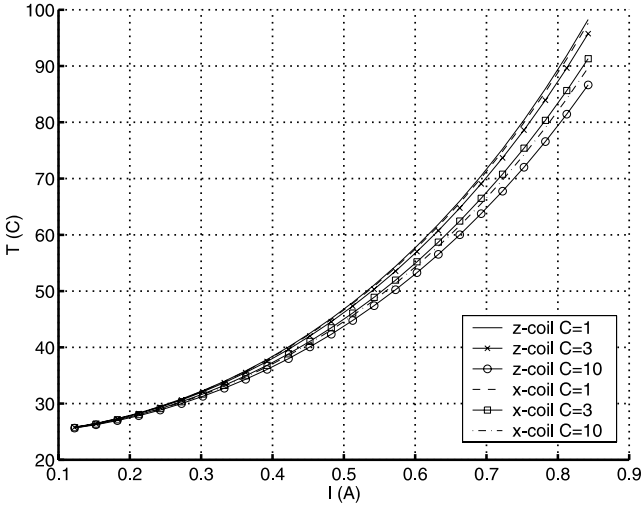

Fig. 4. Temperature of inner layer of four-layer z-coil and x-coil as a function of current, designed for cooling coefficient ratios of $C = 1$, $C = 3$, and $C = 10$ in each case. For both sets of coils, values of $h_2 = 36\,\mathrm{W\,m^{-2}\,K^{-1}}$, $h_2' = 0\,\mathrm{W\,m^{-2}\,K^{-1}}$, and $k_{\mathrm{epoxy}} = 0.45\,\mathrm{W\,m^{-1}\,K^{-1}}$ were used.

represents the coil designed without cooling weighting ($C = 1$), the middle line is that with $C = 3$, and the lower line is for $C = 10$. Increasing C, which results in more current being placed close to the coil's more strongly cooled outer surface, leads to a reduction in the temperature of the inner layer. Curves showing the equivalent performance of a set of x-gradient coils, shown on the same figure, can be seen to mirror the behaviour of the z-gradient coils, with the temperature of the $C = 10$ weighted coil being lower than that of the $C = 3$ coil, which is lower than the coil designed using $C = 1$.

In a real experiment, the usable gradient strength may be limited by temperature considerations. If a temperature limit of 80 °C is set, for example, then the unweighted z-coil can be used at a gradient strength of $0.132\,\mathrm{T\,m^{-1}}$, for a 100% duty cycle. In comparison, the $C = 3$ and $C = 10$ weighted coils can be run with progressively higher gradient strengths of 0.133 and $0.149\,\mathrm{T\,m^{-1}}$, respectively. It is noted that although the best increase in performance here is only 16%, between the unweighted coil and the $C = 10$ weighted coil, this useful increase is achieved at no significant cost in terms of other coil parameters, as can be seen in Table 1. Indeed, the coil performance in some respects, such as the efficiency and shielding, is significantly enhanced. The inductance is 20% higher, but the value of 39.5 μH does not pose a significant limit on gradient risetime.

Tables 3 and 4 summarise the characteristics of the shielded z- and x-coils with varying numbers of layers. The coils were designed using cooling coefficient ratios of $C = 1$ and $C = 3$. It can be seen that as the number of layers increases, the usable wire diameter also increases. Consequently, a greater number of wires can be used to achieve the target resistance, and the coil's efficiency also increases. However, because of this, the coil's inductance also increases for larger numbers of layers. It can also be

Table 3
Summary of key parameters for shielded, multi-layer, z-coils with various numbers of layers, $C = 1$ and $C = 3$ cooling weighting, and a conventional unweighted, two-layer shielded coil

	Two-layer	Five-layer		Eight-layer	
	Conventional	$C = 1$	$C = 3$	$C = 1$	$C = 3$
Average shielding	4.711%	5.617%	2.909%	7.877%	1.386%
Efficiency ($\mathrm{T\,m^{-1}\,A^{-1}}$)	0.174	0.199	0.201	0.252	0.253
Inductance (μH)	28.39	43.18	45.67	71.68	75.16
Resistance (Ω)	1.86	2.00	1.91	2.00	1.87
No. of wires/layer	32, 7	27, 12, 4 4, 9	23, 14, 9 3, 12	22, 15, 9, 6 2, 3, 6, 8	20, 14, 10, 8 6, 2, 6, 12
Wire diameter (μm)	251	303	329	346	380

Table 4
Summary of key parameters for shielded, multi-layer, x-coils with various numbers of layers, $C = 1$ and $C = 3$ cooling weighting, and a conventional unweighted, two-layer shielded coil

	Two-layer	Five-layer		Eight-layer	
	Conventional	$C = 1$	$C = 3$	$C = 1$	$C = 3$
Average shielding	0.540%	1.289%	1.232%	3.092%	1.321%
Efficiency ($\mathrm{T\,m^{-1}\,A^{-1}}$)	0.132	0.142	0.149	0.165	0.177
Inductance (μH)	34.12	43.42	50.05	62.15	76.93
Resistance (Ω)	2.03	1.93	2.01	1.82	1.91
No. of wires/layer	29, 7	22, 11, 4, 3, 9	21, 12, 7, 1, 12	18, 13, 8, 5, 02, 5, 8	17, 13, 10, 7 4, 1, 5, 12
Wire diameter (μm)	301	370	381	423	444

seen that in all cases, increasing the ratio of the outer to inner cooling coefficients from 1 to 3 improves the shielding, as has already been noted for the four-layer coils.

Increasing the number of layers has the effect of spreading out the current distribution over a larger usable volume. Consequently, the number of turns in each layer decreases. The result of this is that the shielding effectiveness is decreased as the number of layers increases. This is due to a higher level of mismatch between the ideal continuous current and the discretised representation, as has already been discussed as one of the effects seen when varying the cooling coefficient ratio.

The conventional coils with a single primary layer and a screen were found to have significantly lower efficiency than the multi-layer coils, confirming that higher performance screened gradient coils can be designed via the multi-layer approach, when coil resistance is the limiting factor. For five- and eight-layer z-coils, increases in efficiency of up to 1.16 and 1.45 times respectively are observed in Table 3. The equivalent ratios for the x-coils presented in Table 4 are 1.13 and 1.34.

4.2. Experimental

The fit between the modelled and experimental temperature measurements is shown in Fig. 5. Here, the points represent the experimental measurements on the four layers of the real coil operating with natural convection air-cooling. The lines represent the modelled data for layers one, two, three and four of the coil. The data were fitted by varying the values for the thermal conductivity of the epoxy resin and the heat transfer coefficient of the outer surface. The best fit was given by a value for the thermal conductivity of $0.45\,\mathrm{W\,m^{-1}\,K^{-1}}$ for the epoxy resin, while the best value of the outer surface heat transfer coefficient was $36\,\mathrm{W\,m^{-2}\,K^{-1}}$. Both of these values are reasonable. The thermal conductivity lies within the range of typical thermal conductivities for epoxy resins of 0.17–$0.87\,\mathrm{W\,m^{-1}\,K^{-1}}$ [15], and typical values of natural convection coefficients for air would lie in the range 1–$60\,\mathrm{W\,m^{-2}\,K^{-1}}$[19]. The model can be seen to agree quite well with the observed experimental data if these particular values are adopted, and all experimental values lie within $0.7\,^{\circ}\mathrm{C}$ of the modelled curves.

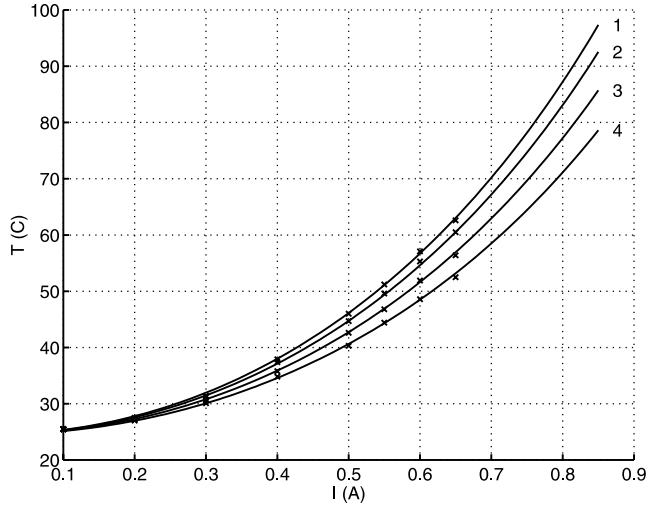

Fig. 5. Experimental temperature measurements with predicted temperatures from model for four-layer $C = 3$ weighted z-coil.

The resistance and inductance of the coil that was built were measured using an LCR meter. The resistance was measured to be $4.5 \pm 0.1\,\Omega$ which compares with an expected value of $4.456\,\Omega$ from the design parameters, allowing for the factor of two from the use of a different wire-gauge. The inductance was measured to be $37 \pm 1\,\mu\mathrm{H}$, compared with a predicted value of $33.61\,\mu\mathrm{H}$. The higher inductance of the real coil can be accounted for by the presence of the lead-in wires for the individual layers and also the connecting leads to the LCR meter.

It should be noted that in the construction of this coil, the optimum wire-diameter was not used. The effect of this is that although in terms of efficiency and field performance the characteristics reliably describe a coil of this particular geometry, the resistance is considerably higher than would have been expected. The tabulated data represents the coils as they were originally designed, before the change in wire-gauge was adopted. In drawing comparisons between the various four-layer coil designs, and between the theoretical and experimental data, the altered wire-gauge was accounted for in all theoretical coils by doubling the resistivity of the current-carrying conductors. Consequently, more realistic coils would be expected to be usable at higher gradients than indicated here before reaching the temperatures suggested by these results.

It should also be noted that in order to allow space for the temperature sensors between each layer, it was necessary to use a larger than normal layer spacing in the four-layer coils. Again, as a result, the performance of the four-layer coils cannot be considered as optimal for a typical multi-layer gradient coil of this size. A more optimal layer separation was used in the coils presented in Tables 3 and 4, and consequently these coils are more representative of the achievable performance of multi-layer coils.

Results from the experimental field measurements using the four-layer z-coil indicate a significant reduction of the field in a ROI located immediately outside the coil surface. The shielded field had an average magnitude of 6.5% of that produced by the unshielded coil when both coils generate the same internal field gradient. Ideally the measurements would have been made with a four-layer unshielded coil of equivalent geometry to the shielded coil, but no such coil was available. The inner layers will have predominantly

gradient producing characteristics, whereas the outer layers will provide a significant contribution to the shielding. Therefore, driving the inner-most layer was the closest approximation that could be made to an unshielded coil, although the external field will be less than would be expected from a four-layer unshielded coil. As a consequence, the shielding performance will be worse than expected from a comparison of shielded and unshielded four-layer coils. A Biot–Savart field calculation carried out using the inner-most layer as an unshielded coil yielded a theoretical shielding performance of 6.7%, which is in good agreement with the value measured experimentally.

5. Conclusions

It has previously been shown that a multi-layer approach allows the design of gradient coils that yield higher efficiencies and gradient strengths than conventional coils [4,13]. This work has illustrated that the gains can still be realised on the inclusion of active screening. Cooling is also an important parameter for multi-layer coils, and a new method for designing coils with optimal cooling characteristics has been described here. A clear benefit of this method is that higher gradient strengths can be used before a given temperature is reached within the coil. Further, an added benefit of the method is that it can lead to improved shielding performance upon discretisation of the continuous current. A shielded, four-layer, z-coil has been built to verify the performance of both the coil and the model.

The model presented in this work possesses many short-comings if one is aiming for an accurate assessment of the localised temperature variations present in an operational gradient coil. However, this model was not developed to perform such a task, rather it was devised to allow the design of coils in which the current distribution within the coil is weighted to take account of the radial position of the layers and also the relative ease of cooling the coil at each individual surface. For example, when working with small-bore gradient sets for use in animal MRI or MR microscopy, there is often more space available to provide cooling at the outer surface of the coil than at the inner surface, and as such it is preferable to be able to direct the current into radial positions where the heat generated can be more easily removed. The results presented here suggest that the model was successful in this respect.

The immediate intention for future work is to develop a formalism allowing x, y, and z gradient coil layers to be interleaved, thus enabling the design and construction of an integrated multi-layer, screened, three-axis coil. A further direction for future work relating to heat-transfer will be to re-write the mathematical formalism such that the current density is no longer represented as a sum of continuous Fourier harmonics within each layer, but rather to break each layer into a number of adjacent, isothermal, current rings. Boundary conditions between the rings would ensure current continuity and could be used to model heat flow along the layer. An extra dimension will then have to be added to the sums for equations presented in the theory section for the field, etc., which will result in a slightly longer computing time, particularly as the number of rings is increased to more closely map the temperature variation. The reward for this would be the ability to calculate a pseudo-localised temperature dependence in order to address the issue of thermally optimising the current distribution within the individual layers, rather than just across the layers as a whole. The model will still not be able to consider the azimuthal temperature variations that will occur in transverse gradient coils, but to incorporate these would require a significant increase in the complexity of the design method, and may well be best considered using a finite-element approach rather than the analytical approach detailed here-in.

Acknowledgments

We thank the workshop staff at the Centre for Magnetic Resonance, University of Queensland (UQ), for constructing the gradient coil; Dan Green at the University of Nottingham (UofN) for discussions and assistance with computer programming; Ian Thexton (UofN) and Walter Köckenberger (UofN) for assistance with preliminary investigations; Daniel Barnes (UQ) for assistance with graphics. J.L. is supported by a studentship from the University of Queensland.

References

[1] R. Turner, Minimum inductance coils, J. Phys. E 21 (1988) 948–952.
[2] C.J. Rofe, J. Van Noort, P.J. Back, P.T. Callaghan, NMR microscopy using large, pulsed magnetic-field gradients, J. Magn. Reson. B 108 (1995) 125–136.
[3] P.T. Callaghan, J. Stepisnik, Spatially-distributed pulsed gradient spin echo NMR using single-wire proximity, Phys. Rev. Lett. 75 (1995) 4532–4535.
[4] R. Bowtell, P. Robyr, Multi-layer gradient coil design, J. Magn. Reson. 131 (1998) 286–294.
[5] P. Mansfield, B. Chapman, Active magnetic screening of coils for static and time dependent magnetic field generation in NMR imaging, J. Phys. E 19 (1986) 540–545.
[6] R. Bowtell, P. Mansfield, Screened coil designs for NMR imaging in magnets with transverse field geometry, Meas. Sci. Technol. 1 (1990) 431–439.
[7] R. Turner, Electrical coils, US Patent No. 5,289,151, 1994.
[8] J.W. Carlson, K.A. Derby, K.C. Hawrysko, M. Weiderman, Design and evaluation of shielded gradient coils, Magn. Reson. Med. 26 (1992) 191–206.

[9] P.B. Roemer, J.S. Hickey, Self-shielded gradient coils for nuclear magnetic resonance imaging, US Patent No. 4,737,716, 1988.
[10] R.W. Brown, Sh.M. Shvartsman, Supershielding: confinement of magnetic and electric fields, Phys. Rev. Lett. 83 (1999) 1946–1949.
[11] L.K. Forbes, S. Crozier, A novel target-field method MR shim coils: Part 3: Shielded zonal and tesseral shims, J. Phys. D 36 (2003) 68–80.
[12] B.A. Chronik, B.K. Rutt, Constrained length minimum inductance gradient coil design, Magn. Reson. Med. 39 (1998) 270–278.
[13] J. Leggett, S. Crozier, S. Blackband, B. Beck, R. Bowtell, Multilayer transverse gradient coil design, Concepts Magn. Reson. B 16 (2003) 38–46.
[14] D.C. Alsop, T.J. Connick, Optimisation of torque-balanced asymmetric head gradient coils, Magn. Reson. Med. 35 (1996) 875–886.
[15] CRC Materials Science Handbook, third ed., CRC Press, Boca Raton, 2001.
[16] CRC Handbook of Chemistry and Physics, 78th ed., CRC Press, Boca Raton, 1997.
[17] F.J. Keller, W.E. Gettys, M. Skove, Physics—Classical and Modern, second ed., McGraw-Hill, New York, 1993.
[18] L.C. Thomas, Heat Transfer—Professional Version, second ed., Capstone Publishing Corporation, 1999.
[19] A.J. Reynolds, Thermofluid Dynamics, Wiley-Interscience, 1971, p. 500.